Reconstruction of Reduced-Dose SparseCT Data Acquired With An Interrupted-Beam Prototype On A Clinical Scanner

Matthew J. Muckley, Baiyu Chen, Thomas O'Donell, Matthias Berner, Thomas Allmendinger, Karl Stierstorfer, Thomas Flohr, Bernhard Schmidt, Aaron D. Sodickson, Daniel K. Sodickson, and Ricardo Otazo

***Abstract*—Low-dose X-ray CT is a rapidly-advancing area in medical imaging. A number of paradigms for low-dose CT have emerged, some of which are based on sparse sampling. Sparse sampling approaches using view-based subsampling have been limited to simulations due to difficult hardware implementation, but recently a more practical within-view sparse sampling approach was proposed called SparseCT. SparseCT operates by interrupting the source beam with a multislit collimator before it reaches the patient, thus creating a row-subsampled projection view. By programming the multislit collimator to move throughout the scan, undersampling is possible in both the row and the projection angle dimensions. Here we develop reconstruction algorithms tailored to the interrupted-beam acquisition to compensate for partial source obstruction and nonideal statistical weighting. We present reconstruction of phantom data acquired with the first multislit collimator prototype on a clinical scanner using simulated motion patterns.**

I. Introduction

X-ray CT is currently one of the most important diagnostic tools available in the clinic. However, the ionizing radiation dose of CT remains a risk to patients, particularly pediatric patients and those with chronic illnesses. Thus, radiation dose reduction is an engaging topic of research in the CT field. A number of approaches have been proposed for reducing radiation dose in CT. The most common approach is to reduce the tube current. Iterative reconstruction techniques that compensate for the increased noise have been promising areas of research, with successful commercial examples such as ADMIRE [1] and research examples based on iterative algorithms with edge-preserving regularizers [2].

M. J. Muckley, B. Chen, and D. K. Sodickson are with the NYU School of Medicine, New York, NY.

T. O'Donnell, M. Berner, T. Allmendinger, K. Stierstorfer, T. Flohr, and B. Schmidt are with Siemens Healthineers.

A. D. Sodickson is with Harvard Medical School, Boston, MA.

R. Otazo is with the Memorial Sloan-Kettering Cancer Center, New York, NY.

An alternative approach to tube-current reduction is sparse sampling. These techniques show promise because they can be combined with standard compressed sensing theory [3]. This allows extremely high dose reductions. A practical way to achieve sparse sampling is to partially block the X-ray beam. This method, called SparseCT or interrupted-beam CT, has gained interest since it can achieve sparse sampling by using a multislit collimator (MSC) in replacement of the standard source collimator on current clinical systems [4]. Contrary to sparse-view sampling approaches that block entire views, SparseCT achieves sparse sampling within views. A number of aspects of SparseCT have already been studied in simulation. These discovered that penumbra effects can modify the noise level in the acquired sinogram [5]. The increased noise can be compensated for by using larger slits with larger spacings, and these have been observed to lead to only a modest drop in incoherence [6]. Nonetheless, none of these studies were done using real-world data.

In this work, we demonstrate the reconstruction of phantom data acquired using the first SparseCT MSC on a clinical scanner. The SparseCT collimator has four open rows out of every 16 (W4S16). We collect data while holding the MSC in 16 different static positions. We then retrospectively stitch the positions together to create a synthetic, linear motion pattern. We show new features that the proposed sampling scheme applies to the sinogram, including that of partial source obstruction. We outline a new reconstruction pipeline for the prototype, which includes modifications that take into account these new features. The images constitute the first demonstration of SparseCT using real-world data.

II. Methods

A. Prototype Design and Data Acquisition

SparseCT calls for an interrupted-beam scanner design. The ideal design is to apply a binary sampling

mask along the row dimension of the sinogram. During the scan, the MSC would be jittered along the z direction throughout a helical scan, giving incoherent θ-z undersampling. We desire incoherence in the acquisition to improve the performance of sparsity-promoting reconstruction as predicted by compessed sensing theory.

Such a design requires building a multislit collimator (MSC) to interrupt the X-ray beam prior to reaching the patient. Fig. 1 shows a schematic of such a design. The

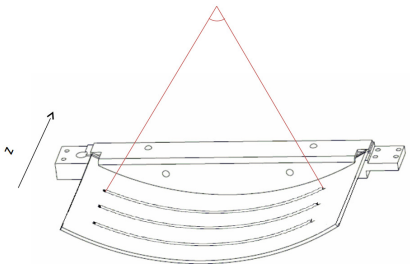

Fig. 1: Schematic of a multislit collimator (MSC) and source with periodic slit openings. In the W4S16 design, each slit illuminates four rows of the detector, and the repetition period is 16 detector rows.

design places the MSC into the gantry in place of the normal source collimator.

A number of parameters can govern the construction and operation of the MSC. Designing the MSC so that it has more, thinner slits produces more incoherence in the sampling pattern [6] at the cost of reduced dose efficiency due to penumbra effects [5]. To balance this tradeoff, we opted for a W4S16 scanner design, which exposes 4 detector rows out of every 16 in the ideal binary mask case. In reality, due to the penumbra, each slit illuminates more than 4 rows at a reduced intensity, but the W4S16 represents a balance point between these effects based on previous simulations [5], [6].

Data were acquired on a SOMATOM Force Scanner (Siemens Healthineers, Forccheim, Germany) with the MSC replacing the normal source collimator. The data were acquired with the MSC being located at 16 different static positions. We used a separate air scan to calibrate the incident flux into the bore of the scanner prior reaching the patient. After standard clinical preprocessing, we synthesized a data set with a moving MSC by retrospectively stitching together the 16 MSC positions. The final data set simulated a linear motion of the MSC from position 1 to position 16 over a single axial rotation. We designate the output of these preprocessing steps as $\mathbf{y}$, the data used for reconstruction.

B. Reconstruction

For reconstruction, we adopted an iterative approach that solves the following optimization problem:

$$\hat{\mathbf{x}} = \underset{\mathbf{x}}{\operatorname{argmin}} \frac{1}{2} \|\mathbf{y} - \mathbf{A}\mathbf{x}\|_{\mathbf{W}}^2 + \beta \sum_{m=1}^{M} \psi\left([\mathbf{C}\mathbf{x}]_m\right), \quad (1)$$

where $\mathbf{x}$ is the image volume to be reconstructed, $\mathbf{y}$ is the preprocessed sinogram data, $\mathbf{A}$ is a Siddon line projector [7] incorporating sampling patterns and scanner geometry, $\mathbf{C}$ is a finite difference operator, and β is a regularization parameter. The quadratic term in this cost function enforces data consistency, and the regularizer promotes edge sparsity with β determining the level of regularization. $\psi(t)$ is a potential function that we define as the hyperbola function:

$$\psi(t) = \delta^2 \left[\sqrt{1 + (t/\delta)^2} - 1\right]. \quad (2)$$

This potential function makes the regularizer behave analogously to "corner-rounded" Total Variation.

$\mathbf{W}$ is a diagonal matrix constructed of elements w_n, $n \in [1, ..., N]$. We calculated the weights as $w_n = (b_n)^{0.5}$, where b_n is the nth prelog sinogram data point. This is a balanced method that preserves some of the noise mitigation benefits of reducing emphasis on low-signal projections [8] without giving too much weight to a small number of projections [9]. We solved (1) with the ordered subsets with momentum algorithm [2].

C. Partial Source Obstruction

Solving the problem in (1) requires building a routine that can apply $\mathbf{A}$ and $\mathbf{A}^T$, the forward and back-projection operations. We used the Siddon line integral method [7]. This method draws rays between the source location and each detector location. In normal settings, the source is approximated as a point source for such methods, but the insertion of the MSC partially obstructs the source. Thus, the assumed point source center no longer corresponds to the observed source center - effectively, a row-dependent shift in the source location. To precompensate for this effect, we simulated what portion of the source would be observable for each row of the detector. Then, we jitter the source location in the $\mathbf{A}$ operator during reconstruction. A schematic of this process is shown in Fig. 2. For each row of the detector, the assumed point source location is jittered based on the centroid of the observable portion of the detector. To do this, we approximated the source as a summation of Gaussian blobs of varying intensity, and then simulated how much of the source would be occluded in each row of our design geometry.

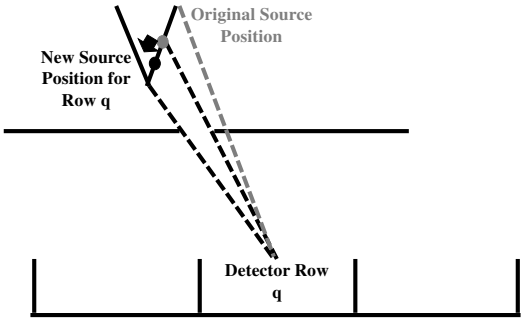

Fig. 2: Schematic of partial source obstruction. In the absence of the MSC, the assumed point source location for detector row q would correspond to the true source centroid. However, in the presence of the MSC, the observed centroid is shifted. This shift was applied to each of the ray casting steps in calculating $\mathbf{A}$.

III. Results

A. Partial Source Obstruction

Fig. 3 shows sinograms of an American College of Radiology (ACR) phantom acquired with and without the multislit collimator (MSC). The phantom has inserts that travel straight along the length of the phantom, as can be seen in the sinogram in Fig. 3a. When the MSC is inserted, the effects of partial source obstruction lead to a varying cone beam magnification in the row direction in Fig. 3b. The shift is most observable in slanted line patterns where the operating table is located in the sinogram.

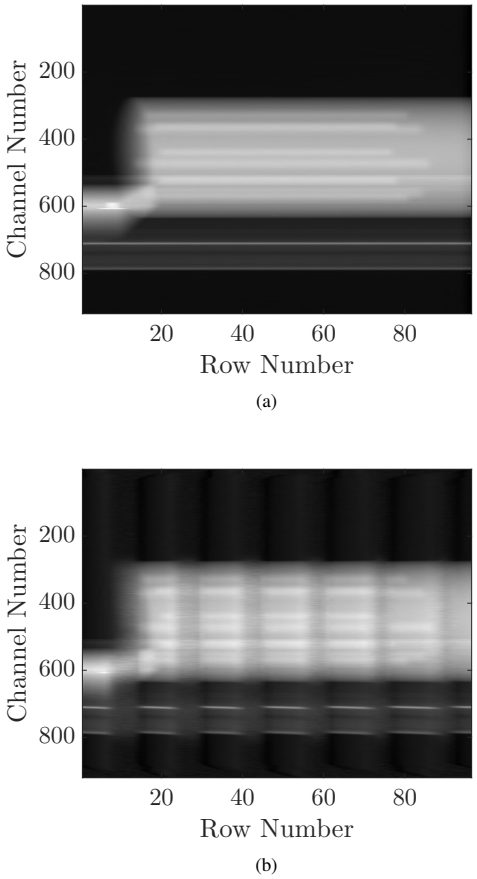

Fig. 3: Effects of partial source obstruction on one projection view. (a) shows the artifact-free ACR phantom with an open collimator, while (b) shows how a shift-variant magnification results with the MSC, most easily observed in the slanted lines of the operating table.

To correct for partial source obstruction, we applied the technique outlined in Section II-C to a scan in which the MSC position was fixed. This means that parts of the object where the MSC was fully opened were fully sampled, and we should observe no subsampling artifacts. Prior to partial source obstruction correction, some areas are enlarged and others are diminished. Fig. 4 shows the effect of the partial source obstruction correction. The corrected version of the phantom is shown in Fig 4a, while the uncorrected version subtracted from the corrected version is shown in Fig. 4b. The dark outline around the edge of the ACR phantom implies that the uncorrected reconstruction was spatially diminished in this slice.

B. Linear Motion

Fig. 5 compares results with an open collimator vs. the MSC with linear motion by zooming in on the 7 lp/com insert of the ACR phantom. The open collimator result was obtained with the standard Siemens FBP pipeline. Some degradation occurs around the edge of the bar resolution pattern of the MSC image in Fig. 5d. Nonetheless, the reconstruction with the MSC while simulating linear motion is able to gain similar resolution to the fully-open, ideally sampled case. When no motion is applied, significant image degradation is observable in penumbra regions (not shown).

IV. Discussion

We have demonstrated reconstruction with an interrupted-beam CT prototype with simulated linear

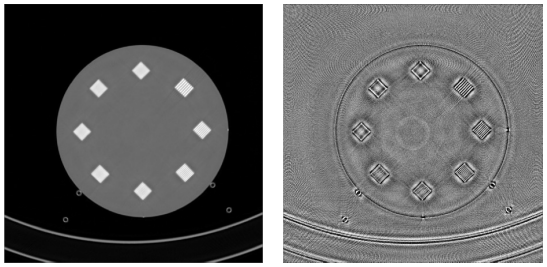

(a) (b)

Fig. 4: Effects of partial source obstruction. (a) shows the corrected image (-1000 HU to 1400 HU), while (b) shows the original uncorrected image subtracted from the corrected (-100 to 100 HU), demonstrating that the original image was minimized in this slice.

motion. We showed that the beam interruption can introduce new partial source obstruction effects and proposed a means to correct for them. We observed that this correction could change the size of the phantom in various slices. Subjectively, some blurring also occurred with the use of partial source obstruction correction - possibly due to incorrect assumptions on the source intensity distribution in our simulations. In the future, we aim to get accurate measurements of the source intensity distribution to improve this correction process.

Fig. 5 shows that SparseCT with a 4-fold dose reduction and linear motion can attain similar resolution to the standard full-dose case using the ACR phantom, which demonstrates practical sparsity-based dose reductions on a clinical scanner. Our results without any motion (not shown) indicated that moving the MSC throughout the acquisition is essential to preserving image quality. Without motion, significant image degradation is observable in the penumbra regions. In the future, we will perform reconstructions on cases involving real-world motion. This will require new advances in registering the air calibration to various motion states, as well as further developing the partial source obstruction model to handle motion states that are not explicitly simulated.

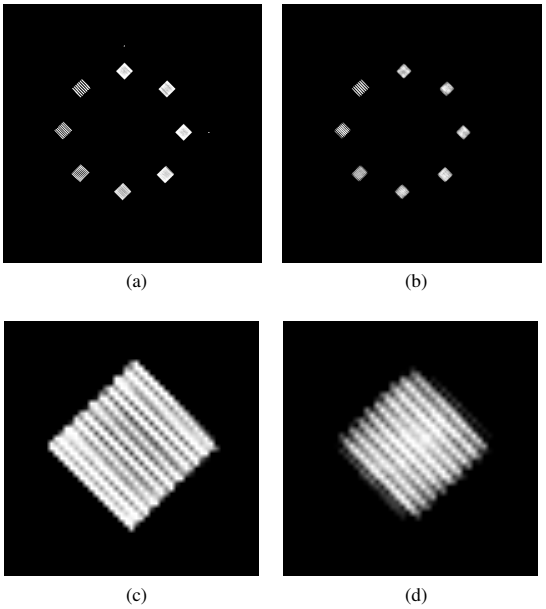

(a) (b) (c) (d)

Fig. 5: Reconstructions of the ACR phantom with an open collimator vs. linear motion (900 HU to 1100 HU window). (a) reconstructed ACR slice with standard acquisition and reconstruction, with (c) showing a zoomed-in version of the 7 lp/cm insert. (b) reconstructed 7 lp/com insert with 4-fold reduction (W4S16 pattern) and linear motion, with (d) showing a zoomed-in version of the third insert. Both methods show similar resolution.

REFERENCES

[1] S. Gordic, F. Morsbach, B. Schmidt, T. Allmendinger, T. Flohr, D. Husarik, S. Baumueller, R. Raupach, P. Stolzmann, S. Leschka, T. Frauenfelder, and H. Alkadhi, "Ultralow-dose chest computed tomography for pulmonary nodule detection: first performance evaluation of single energy scanning with spectral shaping," *Investigative Radiology*, vol. 49, no. 7, pp. 465–73, 2014.

[2] D. Kim, S. Ramani, and J. A. Fessler, "Combining ordered subsets and momentum for accelerated X-ray CT image reconstruction," *IEEE Trans. Med. Imag.*, vol. 34, pp. 167–78, Jan. 2015.

[3] E. J. Candes and M. B. Wakin, "An introduction to compressive sampling," *IEEE Sig. Proc. Mag.*, vol. 25, pp. 21–30, Mar. 2008.

[4] T. Koesters, F. Knoll, A. Sodickson, D. Sodickson, and R. Otazo, "SparseCT: Interrupted-beam acquisition and sparse reconstruction for radiation dose reduction," in *SPIE Med. Im.*, 2017.

[5] B. Chen, M. J. Muckley, T. O'Donnell, A. Sodickson, T. Flohr, K. Stierstorfer, B. Schmidt, F. Knoll, A. Primak, D. Faul, D. Sodickson, and R. Otazo, "Realistic undersampling model for compressed sensing using a multi-slit collimator," in *Proc. Intl. Mtg. on Fully 3D Image Recon. in Rad. and Nuc. Med.*, 2017.

[6] M. J. Muckley, B. Chen, T. Vahle, F. Knoll, A. Sodickson, D. K. Sodickson, and R. Otazo, "Regularizer performance for SparseCT image reconstruction with practical subsampling," in *Proc. Intl. Mtg. on Fully 3D Image Recon. in Rad. and Nuc. Med.*, 2017.

[7] R. L. Siddon, "Fast calculation of the exact radiological path for a three-dimensional CT array," *Med. Phys.*, vol. 12, pp. 252–5, Mar. 1985.

[8] J.-B. Thibault, K. Sauer, C. Bouman, and J. Hsieh, "A three-dimensional statistical approach to improved image quality for multi-slice helical CT," *Med. Phys.*, vol. 34, pp. 4526–44, Nov. 2007.

[9] G. L. Zeng and W. Wang, "Does noise weighting matter in CT iterative reconstruction?," *IEEE Transactions on Radiation and Plasma Medical Sciences*, vol. 1, no. 1, pp. 68–75, 2017.